Check for updates

A VCD study on micro-solvation and self-aggregation of *N*-acetyl tryptophan propylamide

Dilber Tan, [ID] Veronika Stoianova [ID] and Christian Merten [ID] *

The analysis of VCD spectra recorded in hydrogen bonding solvents often requires the explicit consideration of solute–solvent interactions in the DFT-based spectral calculations. While such a micro-solvation approach is straightforward for molecules with a single hydrogen bonding site, the possibility of finding the solute in various solvation states further complicates the analysis for molecules with several donor sites. Herein we analyse the VCD and IR spectra of the small peptide **Ace-Trp-N(*n*-Pr)**, which were recorded in chloroform-d_1, acetonitrile-d_3 and dimethylsulfoxide-d_6, and aim to evaluate how molecular dynamics simulations can support a micro-solvation approach by providing information on the number of simultaneous solute–solvent interactions. The spectra recorded in DMSO-d_6 and ACN-d_3 are well described in the micro-solvation scheme as a mixture of double- and triple-solvated species, and the corresponding MD simulations are found to confirm the derived conformational preferences. Unexpectedly, we found that the results of the analysis of the experimental spectra taken in CDCl$_3$ are not well reproduced by those computed for the monomeric species. In fact, unlike for previously investigated peptides, dimerization has to be considered. The ratio of monomeric and dimeric species could be derived from MD simulations, which also suggested that the most abundant species is an open-chain dimer with indol–N–H$\cdots$O=C$_{acetyl}$ interactions.

Introduction

Studying the effect of solute–solvent interactions is a particular challenge in computational spectroscopy, and especially in computational vibrational circular dichroism (VCD) spectroscopy.[1–3] While strong solute–solvent interactions may lead to conformational changes, and shifts in vibrational frequencies and relative absorption intensities, hydrogen bonding interactions have also been shown to influence the sign of VCD bands.[4] For this reason, when applying VCD spectroscopy for the determination of absolute configurations,[5–7] non- or weakly interacting solvents are preferred over polar protic solvents, as they are typically sufficiently treated using a continuum solvation model.[8,9] However, using VCD spectroscopy to characterize complex molecules in a strongly interacting environment often requires an explicit treatment of the interactions.[10,11] While there are methods to obtain VCD spectra directly from *ab initio* molecular dynamics (MD) and other MD-based approaches,[12–15] these routes are computationally demanding, especially as molecular size increases. Typically, a micro-solvation approach is applied,[10] in which the effect of solute–solvent interactions on conformational preferences and computed spectroscopic

properties is computed by placing explicit solvent molecules near hydrogen bonding sites of the solute. While this approach is usually sufficient for small molecules with a single or spatially well-separated hydrogen bonding sites, solutes possessing several hydrogen bonding sites also capable of forming intramolecular bonds are occasionally challenging to treat. For peptides,[16–19] for instance, it cannot simply be assumed that all hydrogen bonding sites are permanently solvated. Instead, a competition between intra- and intermolecular interactions likely leads to a mixed solvation state with conformers being solvated with different numbers of solvent molecules. In non-polar or non-hydrogen bonding solvents, such solutes tend to dimerize or aggregate to larger clusters. Likewise, accounting for dimerization is an equally challenging task due to the drastically increased conformational space and the need to balance contributions of dimeric structures with one or more intermolecular hydrogen bonds.

In the present study, we investigate the effect of solute–solvent interactions and self-aggregation on the VCD and IR spectra of **Ace-Trp-N(*n*-Pr)** (Chart 1). We address the problem of potentially mixed solvation states by comparing the conformational distributions of static, explicitly solvated structures with results from MD simulations. Based on thorough analyses of trajectories of **Ace-Trp-N(*n*-Pr)** in dimethyl sulfoxide (DMSO) and acetonitrile (ACN), we demonstrate that such a combined approach helps to ensure that the predicted conformational

Ruhr-Universität Bochum, Fakultät für Chemie und Biochemie,
Organische Chemie II, Universitätsstraße 150, 44801 Bochum, Germany.
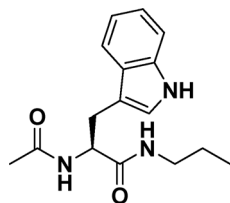*E-mail: christian.merten@ruhr-uni-bochum.de; Web: https://www.mertenlab.de*

Chart 1 Structure of the investigated peptide **Ace-Trp-N(n-Pr)**.

preferences are meaningful. Furthermore, we show that self-aggregation of **Ace-Trp-N(n-Pr)** cannot be neglected in chloroform and how the analysis of an MD trajectory can aid the selection of conformers for spectra predictions.

Experimental and computational details

Synthesis of the target compounds

Enantiopure Ac-Trp-OH (1.00 g, 4.31 mmol) and HOBt·H$_2$O (0.58 g, 4.31 mmol) were dissolved in EtOAc (90 mL) and cooled down to 0 °C. EDC·HCl (0.92 g, 4.73 mmol) was added, and the mixture was stirred for 30 min. n-Propylamine (0.36 mL, 4.31 mmol) and TEA (0.6 mL, 4.31 mmol) were added, and the mixture was stirred for 2 hours after warming to RT. Hexane (20 mL) was added under heavy stirring and stored at +4 °C overnight. The white precipitate was filtered off and washed with EtOAc. The obtained organic layer was washed twice with 1 M HCl (2 × 20 mL), sat. NaHCO$_3$ (3 × 15 mL) and brine, dried over MgSO$_4$, filtered, and evaporated to give the product **Ace-Trp-N(n-Pr)** as a white powder. Yield: 25%. ^{1}H NMR (300 MHz, CDCl$_3$): δ = 8.16 (br s, 1H, indH_1), 7.73 (d, J = 7.68 Hz, 1H, indH_4), 7.37 (d, J = 7.85 Hz, 1H, indH_7), 7.17 (dddd, J = 19.72; 8.15; 7.07; 1.23 Hz, 2H, indH_5, indH_6), 7.05 (d, J = 2.40 Hz, 1H, indH_2), 6.38 (d, J = 7.66 Hz, 1H, AcNH), 5.58 (br s, 1H, n-PrNH), 4.68 (ddd, J = 8.71; 7.67; 5.22 Hz, 1H, C$_\alpha H$), 3.31 (ddd, J = 14.31; 5.23; 0.95 Hz, 1H, C$_\beta$H$'(H)$), 3.11 (dd, J = 15.10; 8.41 Hz, 1H, CβH(H')),), 3.04 (tdd, J = 19.72; 10.36; 3,51 Hz, 2H, n-PrH_1), 1.99 (s, 3H, AcH_2), 1.26 (sexd, J = 36.79; 2.02 Hz, 2H, n-PrH_2), 0.71 (t, J = 7.40 Hz, 3H, n-PrH_3). ^{13}C NMR (75 MHz, CDCl$_3$): δ = 171.32 (C(O)–C$_\alpha$), 170.21 (AcC_1), 136.34 (indC_{7a}), 127.50 (indC_{4a}), 123.15 (indC_2), 122.43 (indC_6), 119.92 (indC_5), 119.03 (indC_4), 111.37 (indC_7), 111.07 (indC_3), 54.25 (C$_\alpha$), 41.34 (n-PrC_1), 28.84 (C$_\beta$), 23.40 (n-PrC_2), 22.55 (AcC_2), 11.27 (n-PrC_3). HR-ESI-MS (ACN): found: 288.8; 320.0; 351.5 m/z calculated: [M + H]$^+$ = 288.2; [M + MeOH + H]$^+$ = 320.2; [M + ACN + Na]$^+$ = 351.2 m/z.

IR and VCD spectroscopy

The IR and VCD spectra were recorded on a Bruker Vertex 70 equipped with a PMA 50 unit for polarization-modulated measurements. Samples were held in BaF$_2$ cells with 50, 100, or 200 μm path length. Concentrations were adjusted so that no IR bands of the sample were above 0.9 absorbance units and are given in the corresponding captions. The IR spectra were accumulated for 32 scans, while the VCD spectra were recorded

over a total measurement time of at least 4 hours each (16 000 scans). The spectral resolution was 4 cm^{-1}. Background correction was carried out by subtraction of the solvent spectrum. The spectra recorded for ACN-d$_3$ and DMSO-d$_6$ solutions are cut below 1100 cm^{-1} due to strong solvent absorbance.

Computational details

If not otherwise mentioned, calculations were carried out for (S)-**Ace-Trp-NMe** as a truncated model of the target compound. The static conformational analysis was carried out by first performing conformational searches using Spartan 14[20] on MMFF[21] level followed by DFT-based geometry optimizations. The so-obtained sets of conformers were complemented by manually generating starting structures for potentially missing conformers. All geometry optimizations and spectra calculations at the DFT-level were performed using Gaussian 09 Rev. E.01[22] at the B3LYP/6-311++G(2d,p) level of theory. Solvation was accounted for implicitly in all calculations by using the IEFPCM[8,9,23] of the respective solvent. Additionally, in the case of ACN-d$_3$ and DMSO-d$_6$, hydrogen bonding to the solvent was considered as discussed in the text. Spectra were simulated by assigning a uniform Lorentzian band shape of 8 cm^{-1} half-width at half-height to the computed dipole and rotational strength. To account for errors due to the harmonic approximation, the computed frequencies were uniformly scaled by a factor σ of 0.98. Note that previous studies[17,18,24] showed that the incorporation of correction terms for dispersive interactions, such as B3LYP-GD3BJ[25] does not lead to an improvement of the spectra and, in fact, rather worsens the match with the experimental data. Therefore, considering the large number of structures that had to be computed to explicitly account for multiple solute–solvent hydrogen bonds, the solute and the solvents, we performed the calculations only at the already established level. Further note that we use the zero-point corrected energies (ΔE_{ZPC}) as a basis for the calculation of Boltzmann weights, and comment on this choice over Gibbs free energies (ΔG_{298K}) in the main text.

The conformational dynamics in bulk solvents were additionally characterized by MD simulations using the Amber 22 software package.[26] The amino acid force field parameters were selected from the ff19SB force field[27] and the solvents were modelled with dedicated all-atom force field parameters for ACN,[28] DMSO,[29] and CHCl$_3$ (as implemented in the Amber package). One solute molecule was placed in a solvent box containing 267 molecules of ACN and 263 molecules of DMSO, while two solutes were placed in 330 molecules of CHCl$_3$. After NVE, NVT, and NPT equilibration at 300 K, production runs were started, and the total trajectory lengths were 130 ns for DMSO, 300 ns for ACN, and 260 ns for CHCl$_3$. In all simulations, a step size of 2 fs was used.

Results and discussion

Compared to previously investigated peptides, the experimental VCD and IR spectra of **Ace-Trp-N(n-Pr)** (Fig. 1) recorded in the
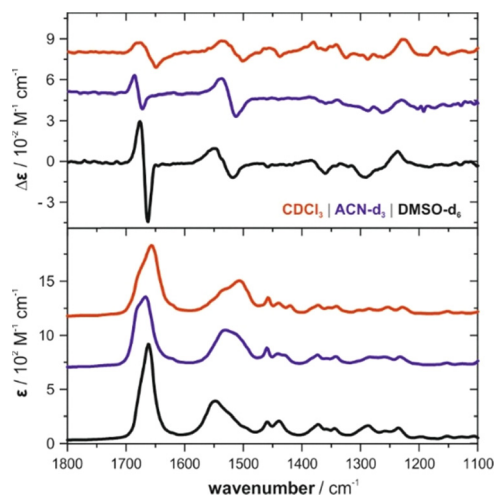
Fig. 1 Comparison of the experimental and computed VCD and IR spectra of (S)-**Ace-Trp-N(n-Pr)** in CDCl$_3$ (0.105 M, 100 μm), ACN-d$_3$ (0.077 M, 200 μm), and DMSO-d$_6$ (0.208 M, 50 μm).
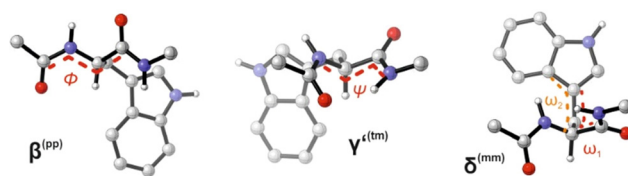

Fig. 2 The lowest energy structures of the β-, γ'-, and δ-families obtained within the IEFPCM of chloroform (non-polar hydrogens, except for the one at the stereocenter, are omitted for clarity). The superscripts indicate the side group conformation as ($\omega_1\omega_2$) with *trans* or positive/negative *gauche* orientation. The conformer $\delta^{(tm)}$ is favoured over $\delta^{(mm)}$ in the IEFPCMs of the polar solvents.

three investigated solvents are remarkably similar. The VCD spectra appear to differ mostly in band widths and relative intensities. It is noteworthy that the amide I signature (1700–1650 cm^{-1}) becomes significantly sharper and more intense with increasing polarity and hydrogen bonding capability of the solvents. In the same order, the amide II and III regions (1600–1500 and 1300–1200 cm^{-1}) also become more defined. Likewise, in the three IR spectra, changes in the shape of the amide I and II bands can be noted. The most significant sharpening of the amide I band appears in DMSO-d$_6$. The amide II band showed notably different band shapes with a blue shift of the maximum in ACN-d$_3$ and DMSO-d$_6$. While the similar shapes of the three VCD spectra may indicate only minor changes to the conformational distribution, the changes in the IR spectra highlight a clear solvent effect on vibrational signatures.

Conformational analysis

As contributions of different conformations of the *n*-propyl chain were considered to average out, the structure **Ace-Trp-N(n-Pr)** was truncated to **Ace-Trp-NMe**, *i.e.*, the *n*-propyl chain was replaced with a methyl group for all calculations. Our systematic conformational search on **Ace-Trp-NMe** explored the peptide backbone angles (ϕ/ψ angles; *cf.* Fig. 2) as well as the rotation of the indole side chain ($\omega_1 = (C^{(=O)}-C^\alpha-CH_2-C_q)$ and $\omega_2 = (C^\alpha-CH_2-C_q-C_q)$). The conformational space with $\phi < 0$ was extensively sampled as structures in this range are usually significantly preferred for *S*-amino acids. In total, we obtained eight conformers for each of the β-, δ- and γ'-families (*cf.* Fig. 2 for the common nomenclature, Table S1 for geometries and energies). Despite several attempts, only one to two conformers in the pp$_{II}$ region were obtained, depending on the IEFPCM model. Further 18 conformers from outside the common regions or with $\phi > 0$ were optimized as well, but as expected, they were found to be much higher in energy (*cf.* Table S2 and Fig. S1). The β$^{(pp)}$-conformer with both side group

dihedral angles ω_1 and ω_2 in *gauche* (+) orientation was found as the lowest energy structure of **Ace-Trp-NMe** (*cf.* Fig. 2). Within the γ'-family, the γ'$^{(tm)}$- is favoured over the γ'$^{(pp)}$-structure. In the δ-family, the preference depends on the IEFPCM with δ$^{(mm)}$ being favoured in chloroform while the polar solvents stabilize the δ$^{(tm)}$ conformer.

Ace-Trp-N(n-Pr) in DMSO

A continuum solvation model for DMSO alone would not be sufficient to reproduce the experimental features,[16–19] as solute–solvent hydrogen bonds influence vibrational frequencies and intensities. Following a micro-solvation approach,[10] we thus recomputed the conformers of **Ace-Trp-NMe** in the presence of one, two or three explicit solvent molecules. For this purpose, we optimized structures with DMSO-d$_6$ molecules placed near the N–H hydrogen bonding donor sites of the solute, *i.e.*, we computed three one-fold, three two-fold, and one three-fold solvated structures for each conformer. Notably, solute–solvent clusters for some conformers could not be optimized, and occasionally, starting structures also converged towards similar solvated structures. When optimized structures differed only in the relative spatial orientation of solvent molecules, solely the lowest energy one was kept for further consideration. For the discussion, 52 single, 31 double, and 13 triple solvated structures were considered. In parallel to the static optimizations, a molecular dynamics simulation was carried out at the ff19SB force field[27] level for the **Ace-Trp-NMe** and with an all-atom force field. From the analysis of a 132 ns MD trajectory, we obtained a free energy diagram (Fig. 3) that showed the β-, pp$_{II}$-, and δ-/α-regions to be highly populated. Evaluation of the individual populations of the basins yielded a conformational distribution of 29.9% β, 40.2% pp$_{II}$ and 26.9 δ (*cf.* Table 1).

It is noteworthy that there was no particularly high barrier separating the β- and pp$_{II}$-basins of the free energy diagram, suggesting that solvation dynamics may easily shift conformers between the two basins. In fact, when projecting the ϕ/ψ-angles of the explicitly DMSO-solvated structures onto the free energy diagram obtained from the MD, the β- and pp$_{II}$-conformers spread over a wide range of ϕ-angles (*cf.* Fig. 3, left), not allowing for a strict classification into conformer families. For this reason, they were subsequently treated as a combined conformer family for the spectra analysis. Based on the
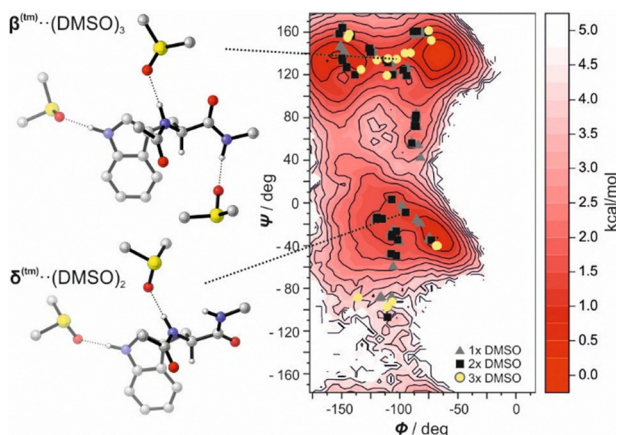
Fig. 3 Free energy diagram from MD simulations indicating the ϕ/ψ-angles of the computed one-, two-, and three-fold solvated conformers in DMSO. $\beta^{(tm)} \cdots (DMSO\text{-}d_6)_3$ and $\delta^{(tm)} \cdots (DMSO\text{-}d_6)_2$ represent the lowest energy double-solvated and triple-solvated structures.

Table 1 Comparison of the distributions over the solvation states **Ace-Trp-NMe**·(DMSO)$_n$ predicted for implicitly (n = 0) and explicitly solvated structures by DFT and extracted from an MD trajectory

	DFT[a]					MD[b]			
Conf.	$n = 0$	$n = 1$	$n = 2$	$n = 3$	Mix[c]	Total[d]	$n = 1$	$n = 2$	$n = 3$
β	41.3	44.8	40.7	95.8	67.8	29.9	4.0	13.0	12.6
pp$_{II}$	0.7					40.2	2.1	12.7	25.3
δ	40.3	40.9	43.6	3.3	22.4	26.9	3.7	13.5	9.3
γ'	16.7	13.1	13.8		8.5	3	0.5	1.7	0.8

[a] Missing percentage is associated with conformers outside the characteristic regions of the Ramachandran plot. [b] Hydrogen bonding criteria: distance (NH⋯O) ≤ 2.7 Å and the angle (N–H⋯O) ≥ 140°. [c] Equal mixture of double and triple solvated states. [d] Difference between the total percentage and the sum over solvated states n = 1.3 is due to a few non-solvated structures.

computed conformer energies, the β/pp$_{II}$-family and δ/α-conformers were populated about equally in the case of the one- and two-fold solvated structures, contributing each with ∼40–45% to the conformational distribution. A minor contribution of ∼10% came from γ'-conformers (*cf.* Table 1 and Tables S3–S5). For the triple-solvated state, however, the contributions of δ-conformers dropped to below 4% and we could not optimize any γ'-geometries with three DMSO molecules. It is a characteristic of δ/α-conformers that the two amide N–H groups are almost parallel. From the lowest energy two-fold solvated structure $\delta^I \cdots (DMSO\text{-}d_6)_2$ (Fig. 3), it can be deduced that these N–H cannot be easily solvated simultaneously by bulky DMSO molecules. In fact, in several structures, a single DMSO molecule was even found in a bifurcated hydrogen bond to both N–H groups. Hence, triple solvation of the δ/α-structures is generally less favourable.

Comparison of the simulated VCD spectra of each solvation state with the experimental data (Fig. 4) revealed that neither one- nor two-fold solvation reproduced the amide I couplet. Only for the triple solvated state, the amide I couplet was found to match in sign. For the amide II region, however, the two-fold
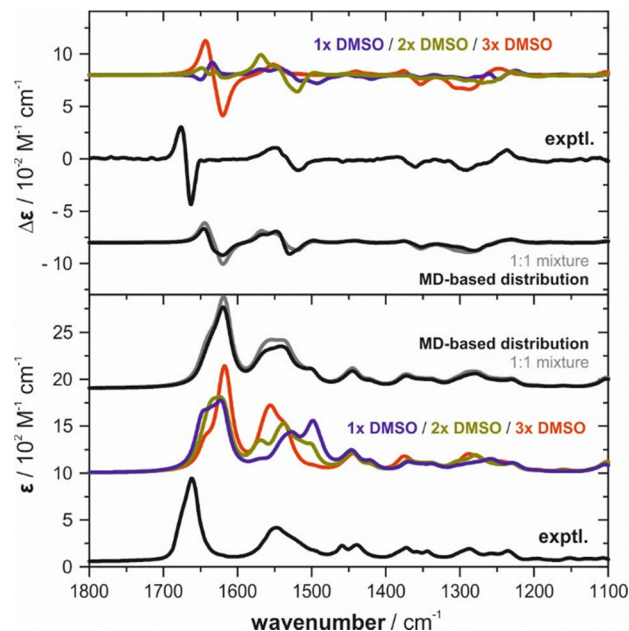

Fig. 4 Comparison of the experimental and computed VCD and IR spectra of (S)-**Ace-Trp-N(n-Pr)** in DMSO-d$_6$ (0.208 M, 50 μm) with computed spectra of the single, double and triple solvated structures, a 1:1 mixture of double and triple solvated state, and an MD-based conformational distribution.

solvated state provided the best match, while the amide III region is again best resembled by the spectra of three-fold solvated structures. A similar observation was made for the amide I and II signatures in the IR spectra. Based on the computed spectral signatures, we thus considered the possibility of a mixture of solvation states. To simulate such a mixed state, we assumed a 1:1 mixture of two- and three-fold solvation (*cf.* Fig. 4), which gave a much better match with the experiment than either of the pure solvation states.

Based on the conformational preferences associated with the pure states, the mixture state consisted of approximately 20% β/pp$_{II}$-, 22% δ-, and 7% $\gamma' \cdots (DMSO\text{-}d_6)_2$ as well as 48% β$\cdots (DMSO\text{-}d_6)_3$. Assuming that each conformer may be present in its fully solvated structure, we also simulated spectra with contributions of 22% δ- and 7% $\gamma' \cdots (DMSO\text{-}d_6)_2$ and 68% β$\cdots (DMSO\text{-}d_6)_3$ (*cf.* Fig. S2 for the underlying conformer family spectra). The spectra of this distribution (not shown) appeared only marginally different from that of the mixed state. Yet, it is important to note that the contributions of each conformer family are almost identical to the numbers derived from the MD analysis (*cf.* Table 1).

In line with our studies on other small peptides,[17–19] an unambiguous decision on the preferred solvation state of each conformer family could not be made within in the micro-solvation approach. Therefore, we analysed the MD trajectory with a focus on the solvation state of a conformer. More specifically, for each snapshot, we determined the conformer family and the number of solute–solvent hydrogen bonds (*cf.* SI for details). Using a maximum S=O⋯H–N distance of 2.7 Å and an angle of >140° as geometric cut-off criteria for the

definition of a hydrogen bond (*cf.* SI for details on the definition of criteria), we found the double- and triple-solvated structures to be about equally likely (*cf.* Table 1). Simulating the VCD and IR spectrum of **Ace-Trp-NMe** by mixing the conformer family spectra with the MD-based ratios of solvation states, also resulted in only marginal changes compared to the 1:1 mixture spectrum (Fig. 4). Hence, in the case of the peptide **Ace-Trp-NMe** in DMSO, the MD simulation cannot be used to further refine the match between the computed and experimental spectra, but they confirmed the general conformational trends.

Ace-Trp-N(*n*-Pr) in ACN

For the simulation of the spectra recorded in ACN, we followed a similar combined approach of micro-solvation and molecular dynamics. As for DMSO, we computed explicitly solvated conformers **Ace-Trp-NMe**$\cdots$(ACN-d$_3$)$_n$. Focussing only on the β/pp$_{\mathrm{II}}$-, δ- and γ′-conformers, we obtained 53 singly, 47 doubly, and 14 triply solvated conformers (*cf.* Tables S6–S8). Interestingly, in contrast to the structural preferences in DMSO, we could optimize notably more ACN-solvated δ-conformers. Furthermore, the β/pp$_{\mathrm{II}}$- and δ/α-conformations of **Ace-Trp-NMe**$\cdots$(ACN-d$_3$)$_3$ were much closer in energy, and both conformer families were predicted to have comparable contributions (Table 2). Apparently, the stick-like structure of ACN causes fewer steric solvent–solvent interactions and allows for a better solvation of δ-structures.

The simulated VCD and IR spectra of the single and double ACN-solvated structures were very similar to those obtained for DMSO (Fig. 5). The shift in the conformational preferences of the triply solvated structures towards the δ-conformers is reflected in a decrease in the intensity of the amide I couplet, which originates from β-structures, and an increase in the amide II signature, that was found to be characteristic for the δ-structures. Hence, unlike for DMSO, the simulated spectra of **Ace-Trp-NMe**$\cdots$(ACN-d$_3$)$_3$ already matched quite well with the experimentally observed band shapes. Nonetheless, as ACN is typically considered a weaker hydrogen bonding acceptor than DMSO, it appeared unlikely that solely triple-solvated structures
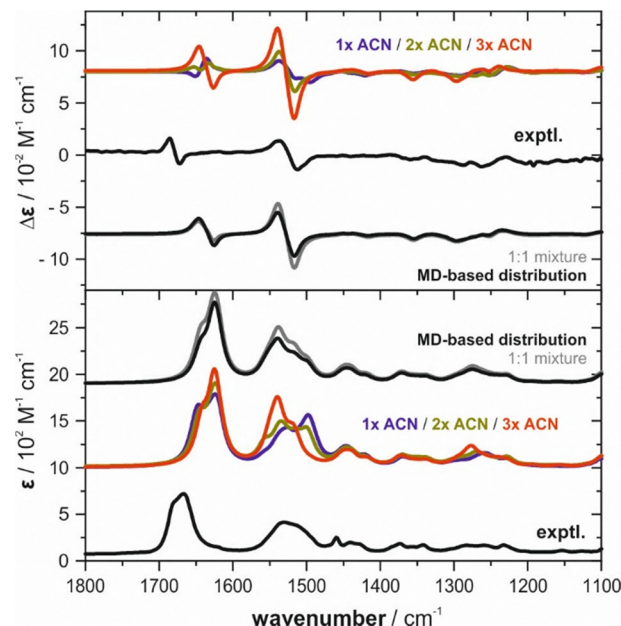

Fig. 5 Comparison of the experimental and computed VCD and IR spectra of (*S*)-**Ace-Trp-N(*n*-Pr)** in ACN-d$_3$ (0.077 M, 200 μm) with computed spectra of the single, double and triple solvated structures, a 1:1 mixture of double and triple solvated state, and an MD-based conformational distribution.

would be populated. Combining the double- and triple-solvated spectra with equal contributions leads to slightly improved relative intensities of the amide I and II regions, further supporting the mixed state hypothesis.

The conformational preferences obtained from the analysis of an MD trajectory of **Ace-Trp-NMe** in ACN[28] agreed nicely with the DFT-computed populations (Table 2, *cf.* Fig. S9 for free energy diagram). It predicted about equal populations of the β/pp$_{\mathrm{II}}$- and δ/α-regions and minor contributions in the γ′-range. To account for the fact that hydrogen bonding of ACN is typically more directional than for DMSO, our analysis of solute–solvent interactions considered the N–H$\cdots$C($\equiv$N) angle as an additional geometric criterium together with the N–H$\cdots$N distance and angle. An ACN molecule was counted as hydrogen bonded to **Ace-Trp-NMe**, when it was found closer than 2.7 Å and with a spatial orientation characterized by an N–H$\cdots$N angle of >130° (*cf.* SI for further details). Under these conditions, the distribution was 32.9%, 45.8%, 18.9% and 2.4% for the triple- to the non-solvated states, respectively. Visual inspection of the simulated VCD and IR spectra based on the underlying distribution of the conformer families (Table 2; *cf.* Fig. S3 for conformer family spectra) shows a minor improvement of the relative intensities compared to the experimental band shapes.

Ace-Trp-N(*n*-Pr) in chloroform

As chloroform can formally be considered a very weak hydrogen bonding donor, it is typically treated as a non-interacting solvent. As demonstrated also in previous studies on peptide solvation,[17–19] it was thus expected that it should be sufficient

Table 2 Comparison of the distributions over the solvation states **Ace-Trp-NMe**$\cdots$(ACN)$_n$ predicted for explicitly solvated structures by DFT and extracted from an MD trajectory

| Conf. | DFT[a] | | | | | MD[b] | | | |
	$n=0$	$n=1$	$n=2$	$n=3$	Mix[c]	Total[d]	$n=1$	$n=2$	$n=3$
β	44.5	48.8	52.9	53.4	53.1	38.6	8.3	17.6	11.4
pp$_{\mathrm{II}}$	0.7					23.0	2.8	9.5	10.4
δ	36.3	37.2	35.3	44.6	40.0	31.9	5.8	15.1	10.3
γ′	17.3	12.6	9.6		4.9	6.5	1.8	3.5	1.0

[a] Missing percentages are associated with conformers outside the characteristic regions of the Ramachandran plot. [b] Hydrogen bonding criteria: distance (NH$\cdots$N) ≤ 2.7 Å, the angle (N–H$\cdots$N) ≥ 130° and the angle (N–H$\cdots$C) deviating by less than 30° from (N–H$\cdots$N). [c] Equal mixture of double and triple solvated states. [d] Difference between the total percentage and the sum over solvated states $n = 1.3$ is due to a few non-solvated structures.

to treat the solvent environment implicitly with a continuum solvation model. Accordingly, we simulated the VCD and IR spectra of **Ace-Trp-NMe** based on implicitly solvated structures (*cf.* Fig. 2, Table S1), with contributions of 55% β/pp$_{II}$-, 29.5% γ′- and 14% δ-conformers. However, the simulated spectra presented a rather unsatisfactory match with the experimental VCD signatures (Fig. 6). The amide I range was predicted with a faint VCD signature, while the experiment clearly showed a strong (±)-couplet.

Exploring the reason for this surprising mismatch, we noted that the spectrum predicted based on ΔG_{298K} gave a good match with the experiment (Fig. S4). This resulted from a change in conformational preferences between the conformer families, mostly caused by the significant increase in the population of the β$^{(tp)}$-conformer. This β$^{(tp)}$-structure had a negligible contribution in the ΔE_{ZPC}-based conformational distribution, and a closer examination revealed a low-frequency vibrational mode (2.9 cm^{-1}) to boost the entropic contribution and to lower the Gibbs free energy of this conformer. Applying entropy corrections[30] or computing the energies and spectra with a different basis set revealed that this stabilization was only coincidental. It nonetheless raised the question, whether the truncation of the propyl group may have affected the conformational distribution. Thus, we recomputed the spectra by considering the full propyl chain and the various possible rotamers. The β-, γ′- and δ-families of conformers grew to 46, 30 and 33 structures, but the overall conformational distribution did not change much: 51.1% β/pp$_{II}$-, 31.6% γ′- and 17.3% δ. For **Ace-Trp-N(n-Pr)**, we obtained essentially the same VCD and IR signatures as **Ace-Trp-NMe** with a slightly more pronounced negative features in the amide II region (*cf.* Fig. 6).
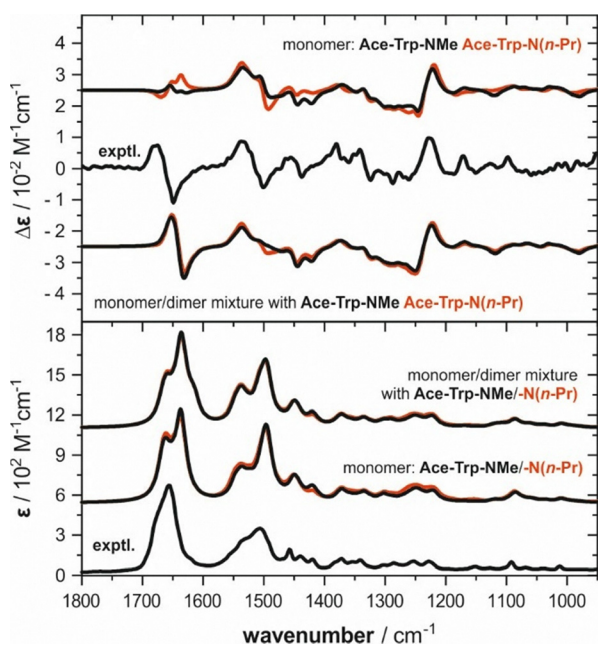
A shoulder to the solvent band at 2244 cm^{-1} indicated hydrogen bonding interactions of the solute to chloroform-d$_1$ (*cf.* Fig. S4). To examine whether interactions with chloroform could induce any significant changes to the conformational distribution or the VCD signatures, we explicitly considered hydrogen bonding interactions with two molecules of chloroform, each interacting with one of the carbonyl groups (C=O···D-CCl$_3$). The influence on conformer weights was again rather small (62% β/pp$_{II}$, 14% δ, 25.5% γ′). Nonetheless, the computed VCD spectrum showed at least an improvement of the amide II region (Fig. 6).

Stronger intermolecular interactions than with chloroform solvent molecules could be expected among **Ace-Trp-NMe** molecules. In fact, the IR spectrum recorded in CDCl$_3$ also showed a broad band near 3305 cm^{-1}, indicating a certain degree of self-aggregation. Dimerization (and even higher aggregation) of **Ace-Trp-NMe** may occur through a variety of bonding patterns. Besides open chain dimers with a single hydrogen bond, also parallel or anti-parallel β-sheet like structures with two hydrogen bonds are possible (Chart S2). Furthermore, symmetric dimer structures with two indole–NH···O=C interactions are possible, which were even found to dominate in the gas phase of Ace-Trp-OMe.[31] This leads to a drastically increased conformational space, and the determination of conformer (family) populations becomes as complicated as for different solvation states.

To explore whether a better match between experimental and computed spectra could be achieved by considering dimerization, we carried out an MD simulation for a simulation box containing two molecules **Ace-Trp-NMe** immersed in 300 molecules CHCl$_3$, *i.e.*, a ratio roughly matching the experimental concentration of 0.1 M. To simplify the analysis of the MD trajectory, we focused only on a distance measure ($d_{C=O···H-N}$ < 3.0 Å) to identify hydrogen bonds. **Ace-Trp-NMe** was found in a non-bound state in about 50% of time, in 34% of the trajectory as an open-chain dimer **(Ace-Trp-NMe)$_2$** with a preference for a single indol–NH···O=C$_{Acetyl}$ interactions, and in an anti-parallel β-sheet structure with two hydrogen bonds between Trp-NH and Trp-C=O in ~12% of the snapshots (Fig. 7). The remaining percentage distributes over other dimeric structures.

Accordingly, the spectra of open-chain and anti-parallel dimeric structures were computed (Fig. S4). The MD simulation predicted the β → β dimers as the most abundant open-chain

Fig. 6 Comparison of the experimental and computed VCD and IR spectra of (S)-**Ace-Trp-N(n-Pr)** in CDCl$_3$ (0.105 M, 100 μm).

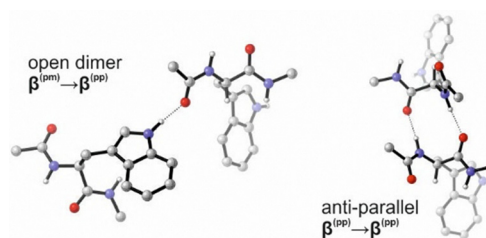Fig. 7 Structures of the lowest energy open-chain and anti-parallel dimer of **Ace-Trp-NMe**.

configuration ($\sim$74%; 18% $\beta \rightarrow \gamma'$, 8% $\beta \rightarrow \delta$). When geometry optimizations were started from structures with γ'- or δ-conformations, the structures mostly reverted to open-chain $\beta \rightarrow \beta$ dimers, $\beta \rightarrow \delta$ were much higher in energy and $\beta \rightarrow \gamma'$ could not be optimized. In line with the results from the MD trajectory analysis, however, we found the six lowest energy structures to be combinations of $\beta^{(pp)}$ and $\beta^{(pm)}$ conformers and to feature indole–NH$\cdots$O=C$_{Acetyl}$ interactions. Structures with the anti-parallel hydrogen bonding pattern optimized towards pairs of β/pp$_{II}$-and γ'-conformers, with the $\beta^{(pp)} \rightarrow \beta^{(pp)}$ dimer being the lowest energy structure of this dimer family (*cf.* Fig. 7, Table S10). The VCD and IR spectra were subsequently simulated by mixing the spectra of monomeric **Ace-Trp-NMe** (50%), the open-chain dimer (34%), and the anti-parallel dimer (12%). The resulting spectra nicely resembled the amide I region, but the amide II region was still lacking the negative component. The negative band of the amide II is present in the spectrum of the open-chain dimers but diminished by the positive contribution from the monomer spectrum (Fig. S4). Certainly, despite the comprehensive conformational sampling, important conformers that could intensify the negative feature may have been overlooked. We note, however, that combining the dimer spectra with the spectra of the full structure **Ace-Trp-N(*n*-Pr)** slightly better resembled the experimental spectra (Fig. 6).[32]

Conclusions

We have presented the experimental VCD and IR spectra of **Ace-Trp-N(*n*-Pr)** recorded in chloroform-d$_1$, ACN-d$_3$ and DMSO-d$_6$. Following a micro-solvation approach, we have shown that double- and three-fold hydrogen-bonded solute–solvent clusters with DMSO-d$_6$ and ACN-d$_3$ need to be considered to reproduce the experimental data. We further demonstrated how MD simulations can be used to refine the molecular picture of solvation by extracting conformer family specific solvation preferences. Although the computed spectra from the qualitative micro-solvation analysis and the more in-depth MD-based interpretation differed only marginally, the presented methodological approach is promising for more flexible solutes. In fact, instead of a full consideration of all solvation states for all conformers, which may be too computationally expensive or time-consuming, it allows for a pre-selection of structures to be computed.

Compared to previous studies,[16–19] the observation that the experimental spectra recorded in CDCl$_3$ could not be reproduced based on a purely implicit solvation through a continuum solvation model was unexpected. Dimerization of the solute had to be considered to obtain a good match with the experiment, which demonstrated that an analysis of VCD spectra can give detailed insights into the solution phase structure of chiral solutes. The fact that neither amide I nor amide II were correctly reproduced by the continuum solvation model stressed that solutes cannot always be treated as isolated molecules in weakly interacting solvents.

Conflicts of interest

There are no conflicts to declare.

Data availability

The data supporting this article have been included as part of the SI. Supplementary information: Structures and energies of computed conformers, additional spectra plots, and analysis of MD simulations. See DOI: **https://doi.org/10.1039/d5cp02728d**.

References

1 J. Bloino, S. Jähnigen and C. Merten, *J. Phys. Chem. Lett.*, 2024, **15**, 8813–8828.
2 P. J. Stephens, F. J. Devlin and J. R. Cheeseman, *VCD Spectroscopy for Organic Chemists*, CRC Press, 2012.
3 L. A. Nafie, *Chirality*, 2020, **32**, 667–692.
4 D. P. Demarque and C. Merten, *Chem. – Eur. J.*, 2017, **23**, 17915–17922.
5 C. Merten, T. P. Golub and N. M. Kreienborg, *J. Org. Chem.*, 2019, **84**, 8797–8814.
6 J. M. Batista Jr, E. W. Blanch and V. da Silva Bolzani, *Nat. Prod. Rep.*, 2015, **32**, 1280–1302.
7 P. L. Polavarapu and E. Santoro, *Nat. Prod. Rep.*, 2020, **37**, 1661–1699.
8 J. Tomasi, B. Mennucci and R. Cammi, *Chem. Rev.*, 2005, **105**, 2999–3094.
9 B. Mennucci, C. Cappelli, R. Cammi and J. Tomasi, *Chirality*, 2011, **23**, 717–729.
10 C. Merten, *Phys. Chem. Chem. Phys.*, 2023, **25**, 29404–29414.
11 C. Merten, *Eur. J. Org. Chem.*, 2020, 5892–5900.
12 K. Le Barbu-Debus, J. Bowles, S. Jähnigen, C. Clavaguéra, F. Calvo, R. Vuilleumier and A. Zehnacker, *Phys. Chem. Chem. Phys.*, 2020, **22**, 26047–26068.
13 S. Jähnigen, D. Sebastiani and R. Vuilleumier, *Phys. Chem. Chem. Phys.*, 2021, **23**, 17232–17241.
14 M. Thomas and B. Kirchner, *J. Phys. Chem. Lett.*, 2016, **7**, 509–513.
15 S. Taherivardanjani, R. Elfgen, W. Reckien, E. Suarez, E. Perlt and B. Kirchner, *Adv. Theory Simul.*, 2022, **5**, 2100293.
16 K. Bünnemann and C. Merten, *J. Phys. Chem. B*, 2016, **120**, 9434–9442.
17 T. Vermeyen and C. Merten, *Phys. Chem. Chem. Phys.*, 2020, **22**, 15640–15648.
18 K. Scholten and C. Merten, *Phys. Chem. Chem. Phys.*, 2022, **24**, 3611–3617.

19 C. Müller and C. Merten, *Phys. Chem. Chem. Phys.*, 2023, **25**, 19462–19469.

20 *Spartan 14*, Wavefunction Inc., Irvine, CA, USA, 2014.

21 T. A. Halgren, *J. Comput. Chem.*, 1996, **17**, 490–519.

22 M. J. Frisch, G. W. Trucks, H. B. Schlegel, G. E. Scuseria, M. A. Robb, J. R. Cheeseman, G. Scalmani, V. Barone, B. Mennucci, G. A. Petersson, H. Nakatsuji, M. Caricato, X. Li, H. P. Hratchian, A. F. Izmaylov, J. Bloino, G. Zheng, J. L. Sonnenberg, M. Hada, M. Ehara, K. Toyota, R. Fukuda, J. Hasegawa, M. Ishida, T. Nakajima, Y. Honda, O. Kitao, H. Nakai, T. Vreven, J. J. A. Montgomery, J. E. Peralta, F. Ogliaro, M. Bearpark, J. J. Heyd, E. Brothers, K. N. Kudin, V. N. Staroverov, T. Keith, R. Kobayashi, J. Normand, K. Raghavachari, A. Rendell, J. C. Burant, S. S. Iyengar, J. Tomasi, M. Cossi, N. Rega, J. M. Millam, M. Klene, J. E. Knox, J. B. Cross, V. Bakken, C. Adamo, J. Jaramillo, R. Gomperts, R. E. Stratmann, O. Yazyev, A. J. Austin, R. Cammi, C. Pomelli, J. W. Ochterski, R. L. Martin, K. Morokuma, V. G. Zakrzewski, G. A. Voth, P. Salvador, J. J. Dannenberg, S. Dapprich, A. D. Daniels, O. Farkas, J. B. Foresman, J. V. Ortiz, J. Cioslowski and D. J. Fox, *Gaussian 09, Rev E.01*, Wallingford CT, USA, 2013.

23 B. Mennucci, J. Tomasi, R. Cammi, J. R. Cheeseman, M. J. Frisch, F. J. Devlin, S. Gabriel and P. J. Stephens, *J. Phys. Chem. A*, 2002, **106**, 6102–6113.

24 K. Bünnemann and C. Merten, *Phys. Chem. Chem. Phys.*, 2017, **19**, 18948–18956.

25 S. Grimme, S. Ehrlich and L. Goerigk, *J. Comput. Chem.*, 2011, **32**, 1456–1465.

26 D. A. Case, H. M. Aktulga, K. Belfon, I. Y. Ben-Shalom, J. T. Berryman, S. R. Brozell, D. S. Cerutti, I. T. E. Cheatham, G. A. Cisneros, V. W. D. Cruzeiro, T. A. Darden, R. E. Duke, G. Giambasu, M. K. Gilson, H. Gohlke, A. W. Goetz, R. Harris, S. Izadi, S. A. Izmailov, K. Kasavajhala, M. C. Kaymak, E. King, A. Kovalenko, T. Kurtzman, T. S. Lee, S. LeGrand, P. Li, C. Lin, J. Liu, T. Luchko, R. Luo, M. Machado, V. Man, M. Manathunga, K. M. Merz, Y. Miao, O. Mikhailovskii, G. Monard, H. Nguyen, K. A. O'Hearn, A. Onufriev, F. Pan, S. Pantano, R. Qi, A. Rahna-moun, D. R. Roe, A. Roitberg, C. Sagui, S. Schott-Verdugo, A. Shajan, J. Shen, C. L. Simmerling, N. R. Skrynnikov, J. Smith, J. Swails, R. C. Walker, J. Wang, J. Wang, H. Wei, R. M. Wolf, X. Wu, Y. Xiong, Y. Xue, D. M. York, S. Zhao and P. A. Kollman, *Amber 2022*, University of California, San Francisco, 2022.

27 C. Tian, K. Kasavajhala, K. A. A. Belfon, L. Raguette, H. Huang, A. N. Migues, J. Bickel, Y. Wang, J. Pincay, Q. Wu and C. Simmerling, *J. Chem. Theory Comput.*, 2020, **16**, 528–552.

28 X. Grabuleda, C. Jaime and P. A. Kollman, *J. Comput. Chem.*, 2000, **21**, 901–908.

29 T. Fox and P. A. Kollman, *J. Phys. Chem. B*, 1998, **102**, 8070–8079.

30 R. F. Ribeiro, A. V. Marenich, C. J. Cramer and D. G. Truhlar, *J. Phys. Chem. B*, 2011, **115**, 14556–14562.

31 A. Gerlach, C. Unterberg, H. Fricke and M. Gerhards, *Mol. Phys.*, 2005, **103**, 1521–1529.

32 Despite this observation, we did not consider the full *n*-propyl chain for the DMSO/ACN-solvated clusters. Anticipating only equally small changes to the VCD signature, potentially also limited to the amide II region, did not seem to justify the additional computational efforts after all.